Biol. Cybern. 85, 65–75 (2001)

Biological Cybernetics

End-point constraints in aiming movements: effects of approach angle and speed

Mary D. Klein Breteler[1], **Stan C. A. M. Gielen**[2], **Ruud G. J. Meulenbroek**[1]

[1] Department of Experimental Psychology, Nijmegen Institute for Cognition and Information, University of Nijmegen, PO Box 9104, 6500 HE Nijmegen, The Netherlands
[2] Department of Medical Physics and Biophysics, University of Nijmegen, The Netherlands

Received: 7 July 1999 / Accepted in revised form: 8 January 2001

Abstract. The present study focuses on two trajectory-formation models of point-to-point aiming movements, viz., the minimum-jerk and the minimum torque-change model. To date, few studies on minimum-jerk and minimum torque-change trajectories have incorporated self- or externally imposed end-point constraints, such as the direction and velocity with which a target area is approached. To investigate which model accounts best for the effects on movement trajectories of such – in many circumstances – realistic end-point constraints, we adjusted both the minimum-jerk and the minimum torque-change model so that they could generate trajectories of which the final part has a specific direction and speed. The adjusted models yield realistic trajectories with a high curvature near movement completion. Comparison of simulated and measured movement trajectories show that pointing movements that are constrained with respect to final movement direction and speed can be described in terms of minimization of joint-torque changes.

1 Introduction

The 'way to approach' a target is an obvious task constraint that may influence the entire trajectory of an aiming movement. Targets can be approached from various angles and with various velocities, which may have consequences for the initial phase of trajectory formation. In previous studies of unconstrained three-dimensional movements it was found that subjects generally strive towards approaching a target area either perpendicularly (Brenner and Smeets 1995; Smeets and Brenner 1999a,b) or at an angle such that occlusion of the target by the hand is avoided (Klein Breteler et al. 1998). To date, trajectory-formation models do not account for the effects that end-point constraints may have on movements, except for the study by Smeets and Brenner (1999a) who modeled grasping movements by means of two minimum-jerk trajectories, one for the thumb tip and one for the finger-tip, both approaching the surface of the object to be grasped perpendicularly. In the present study we therefore investigate the influence of target-approach constraints on aiming movements in detail. The study focuses on two trajectory-formation models, viz., the minimum-jerk model (Flash 1987), according to which movements are planned in a representation of Euclidean workspace, and the minimum torque-change model (Uno et al. 1989), which assumes that movements are planned in joint-torque space. These two models were taken as examples of trajectory-formation models that presume that optimization processes take place in different frames of reference. The models are well known and have a limited number of parameters with which the effect of adding approach constraints can be studied.

In studies on aiming movements, both straight and curved movement trajectories have been reported. Consequently, on the basis of curvature variations of unconstrained movements, no definite conclusion can be drawn as to whether aiming movements are primarily planned in workspace or in intrinsic space. For simple point-to-point aiming movements, which start and end at zero velocity, the principle of jerk minimization yields straight hand paths. Morasso (1981) observed that point-to-point aiming movements indeed tend to be performed along straight paths. Minimum torque-change trajectories, however, show systematic curvature variations, depending on where a particular aiming movement is performed in workspace, as experimentally confirmed by Atkeson and Hollerbach (1985), Uno et al. (1989), Haggard and Richardson (1996), Van Thiel et al. (1998), and Boessenkool et al. (1998). Although it has been demonstrated that curved movements can be accounted for by both models by presuming via points, i.e., intermediate locations through which the hand must move on its way to the predefined end location, it is not clear how these models account for systematic variations

Correspondence to: M. D. Klein Breteler
(Tel.: +31 24 3612628, Fax: +31 24 3616066,
e-mail: kleinbreteler@nici.kun.nl)

in curvature of the trajectory due to self- or externally-imposed end-point constraints such as the angle and speed with which a target area is approached.

Smeets and Brenner (1999a,b) recently added end-point constraints to the minimum-jerk model to investigate how characteristic kinematics of grasping movements can be explained by assuming that in grasping, the finger and thumb follow minimum-jerk trajectories, which are constrained with respect to the approach angle and acceleration. Here we extend their approach and adjust both the minimum-jerk and the minimum torque-change model such that they can also predict movement trajectories of which the final part can be constrained with respect to the velocity direction and amplitude.

In the remainder of this paper we will first discuss the way we implemented the approach constraints in the minimum-jerk and the minimum torque-change model. Subsequently, for both models, the effects of adding the approach angle and speed as constraints on movement trajectories will be investigated. Simulated trajectories will be compared with experimental data obtained from 13 subjects, who were instructed to make horizontal aiming movements under various combinations of approach constraints. More specifically, the participants were asked to approach rectangular target areas sideways and with a particular speed. Under these conditions, the differences between minimum-jerk and minimum torque-change trajectories proved to be substantial according to our simulations. This allowed us to compare the two models in a straightforward manner.

2 Method

2.1 The minimum-jerk model

The minimum-jerk model minimizes

$$C_J = \tfrac{1}{2}\int_0^{t_f} \sum_{i=1}^{n} \left(\frac{\mathrm{d}^3 r_i(t)}{\mathrm{d}t^3}\right)^2 \mathrm{d}t \tag{1}$$

where $r_i(t)$ represents the ith component (of n dimensions) of the vectorial position $\mathbf{r}(t)$ of the end effector, and t_f is the movement time. According to Flash and Hogan (1985) and Flash (1987) a minimum-jerk trajectory, executed in a two-dimensional plane with components $x(t)$ and $y(t)$, is described by two fifth-order polynomials in time:

$$\begin{aligned} x(t) &= C_{0,x} + C_{1,x}t + C_{2,x}t^2 + C_{3,x}t^3 + C_{4,x}t^4 + C_{5,x}t^5 \\ y(t) &= C_{0,y} + C_{1,y}t + C_{2,y}t^2 + C_{3,y}t^3 + C_{4,y}t^4 + C_{5,y}t^5 \end{aligned} \tag{2}$$

where $x(t)$ and $y(t)$ are the x- and y-components of the movement trajectory, respectively, as a function of time t. The values for the six constants $C_{i,x}$ and for the six constants $C_{i,y}$ are determined by six boundary conditions for both the x and y dimension, namely position, velocity, and acceleration, each at the beginning ($t = 0$) and the end ($t = t_f$) of the movement. Smeets and Brenner (1999a) explained the procedure for varying final acceleration in the minimum-jerk model, but with a final velocity of zero. We will show here how the final velocity (for the x- and y-component separately) can also be incorporated in the minimum-jerk model.

The constants $C_{0,\alpha}$ to $C_{5,\alpha}$ have to be calculated for the x- and y-components separately. For example, for the x-dimension they are calculated as follows: For a movement with initial velocity, $V_{0,x}$ (m/s), and initial acceleration, $A_{0,x}$ (m/s^2), equal to zero, $C_{0,x}$, $C_{1,x}$, and $C_{2,x}$ are zero. The values of $C_{3,x}, C_{4,x}$, and $C_{5,x}$ depend on starting position X_0(m), final position X_f(m), movement time MT(s), final velocity $V_{f,x}$ (m/s), and final acceleration $A_{f,x}$(m/s^2). These coefficients are given by:

$$\begin{aligned} C_{3,x} &= \frac{-20X_{0,x} + 20X_{f,x} - 8V_{f,x}\mathrm{MT} + A_{f,x}\mathrm{MT}^2}{2\mathrm{MT}^3} \\ C_{4,x} &= \frac{15X_{0,x} - 15X_{f,x} + 7V_{f,x}\mathrm{MT} - A_{f,x}\mathrm{MT}^2}{\mathrm{MT}^4} \\ C_{5,x} &= \frac{-12X_{0,x} + 12X_{f,x} - 6V_{f,x}\mathrm{MT} + A_{f,x}\mathrm{MT}^2}{2\mathrm{MT}^5} \end{aligned} \tag{3}$$

Similar coefficients are obtained for the y-components by replacing X_0 and X_f by Y_0 and Y_f, respectively. In order to simulate movements with various approach constraints, the values of $C_{i,x}$ and $C_{i,y}$ have to be calculated again for each set of constraints. Note that this results in values for $C_{i,x}$ and $C_{i,y}$, that are constant for each single movement but which will be different for movements with different approach constraints.

2.2 The minimum torque-change model

For calculating minimum torque-change trajectories, the model presented by Uno et al. (1989) was used. The cost function (C_T) is the sum of the squares of the rate of change of torque integrated over the duration of the entire movement:

$$C_T = \tfrac{1}{2}\int_0^{t_f} \sum_{i=1}^{n} \left(\frac{\mathrm{d}T_i}{\mathrm{d}t}\right)^2 \mathrm{d}t \tag{4}$$

where n is the number of joints and T_i is the torque in the ith joint. This cost function has to be minimized and depends not only on the boundary conditions of the movement, but also on the dynamics of the musculoskeletal system.

The torque $\mathbf{T}$ in a two-joint arm satisfies the following differential equations:

$$\begin{aligned} T_1 &= (I_1 + I_2 + 2M_2L_1S_2\cos\theta_2 + M_2L_1^2)\ddot{\theta}_1 \\ &\quad + (I_2 + M_2L_2S_2\cos\theta_2)\ddot{\theta}_2 \\ &\quad - M_2L_1S_2(2\dot{\theta}_1 + \dot{\theta}_2)\dot{\theta}_2\sin\theta_2 + \beta_1\dot{\theta}_1 \\ T_2 &= (I_2 + M_2L_1S_2\cos\theta_2)\ddot{\theta}_1 + I_2\ddot{\theta}_2 + M_2L_1S_2\dot{\theta}_1^2\sin\theta_2 \\ &\quad + \beta_2\dot{\theta}_2 \end{aligned} \tag{5}$$

where T_1 and T_2 represent torques in the shoulder and elbow joint, respectively, and where θ_1 and θ_2 are the

joint angles in shoulder and elbow, respectively. In this equation I_i represents the inertia of limb segment i, M_i is the mass of limb segment i, L_i is the length of segment i, S_2 is the distance of the center of mass of the forearm to the elbow, $\dot{\theta}_i$ is the angular velocity of joint i, and $\ddot{\theta}_i$ is the angular acceleration of joint i.

Since the relationship between C_T and the joint angles as a function of time is nonlinear, the minimum cost $C_{T_{\min}}$ cannot be calculated directly. However, $C_{T_{\min}}$ can be arrived at using an optimization procedure, involving an iterative learning scheme. This will be explained in the following.

The procedure to compute the optimal trajectory with the approach constraints in this study is identical to the procedures outlined by Uno et al. (1989), but is here described in a simpler way that leaves out all details. First a six-dimensional state variable $\mathbf{R}(t)$ and a two-dimensional control variable $\mathbf{u}(t)$ are defined. The state variable $\mathbf{R}(t)$ is a six-dimensional vector representing the two joint angles (the shoulder and elbow), the two joint angular velocities, and the two joint torques at time t. The control variable $\mathbf{u}(t)$ is a two-dimensional vector, which represents the change of the two joint torques per unit of time. It is a measure of the input to the effector-system resulting in a minimum torque-change based movement.

$$\mathbf{R} = \left[\theta_1, \theta_2, \dot{\theta}_1, \dot{\theta}_2, T_1, T_2\right]^{\mathrm{T}} \quad \text{and} \quad \mathbf{u} = \begin{pmatrix} \frac{\mathrm{d}T_1}{\mathrm{d}t} \\ \frac{\mathrm{d}T_2}{\mathrm{d}t} \end{pmatrix} \tag{6}$$

The derivative of the state variable $\mathbf{R}$ with respect to time, needed for calculating the next state $\mathbf{R}(t + \Delta t)$, is both a function of the control variable $\mathbf{u}$ and the state variable $\mathbf{R}$ itself, resulting in the following differential equation:

$$\frac{\mathrm{d}\mathbf{R}}{\mathrm{d}t} = \mathbf{f}(\mathbf{R}, \mathbf{u}) = \left[\dot{\theta}_1, \dot{\theta}_2, \ddot{\theta}_1, \ddot{\theta}_2, u_1, u_2\right]^{\mathrm{T}} \tag{7}$$

At any time $\dot{\theta}_1$ and $\dot{\theta}_2$ are known. $\ddot{\theta}_1$ and $\ddot{\theta}_2$ can easily be calculated as they can be expressed as a function of the joint angles, joint angular velocities, and joint torques (see Appendix A).

The problem now is to find the function $\mathbf{u}(t)$, which gives a minimum for C_T while going from state $\mathbf{R}(t_0)$ to $\mathbf{R}(t_f)$, such that the boundary conditions are met. Solving the differential equation for $\mathrm{d}\mathbf{u}/\mathrm{d}t$ under the constraints of the boundary conditions is hard, since the joint torques T_i depend in a nonlinear way on joint angles, joint velocities, and joint-angle accelerations (see Eq. 5). Instead, the nonlinear differential equation will be solved by variational calculus and dynamical optimization theory. To find the proper $\mathbf{u}(t)$, an auxiliary vector $\boldsymbol{\psi}$ is introduced, which is a six-dimensional vector with the last two components equal to the control variable $\mathbf{u}$. The first four components of $\boldsymbol{\psi}$ are complex functions of the joint angles and their derivatives. As a starting point for the iterative optimization routine, an arbitrary value for $\boldsymbol{\psi}$ suffices. The evolution of $\boldsymbol{\psi}$ in time is described by:

$$\frac{\mathrm{d}\boldsymbol{\psi}}{\mathrm{d}t} = -\left(\frac{\partial \mathbf{f}}{\partial \mathbf{R}}\right)^{\mathrm{T}} \boldsymbol{\psi} \tag{8}$$

The solution of (8) as a function of time gives the optimal joint torques as a function of time for a particular $\boldsymbol{\psi}(0)$. When the joint torques as a function of time are known, the trajectory of the hand as a function of time can be calculated in a straightforward way.

The $\partial\mathbf{f}/\partial\mathbf{R}$ part of (8) is a 6×6 matrix with $(\partial\mathbf{f}/\partial\mathbf{R})_{ij} = (\partial f_i/\partial R_j)$. The calculation of the partial derivatives in the matrix $\partial\mathbf{f}/\partial\mathbf{R}$ is given in Appendix B.

Equation (8) results in a trajectory $\boldsymbol{\psi}(t)$, which minimizes the torque change given the initial value $\boldsymbol{\psi}(0)$. The vector $\mathbf{u}(t)$, which is equal to the fifth and sixth component of vector $\boldsymbol{\psi}(t)$, is then used to calculate $\mathbf{R}(t)$. Different initial values of $\boldsymbol{\psi}(0)$ will result in different trajectories for $\mathbf{R}(t)$. Therefore, we define an error between the desired state $\mathbf{R}_f$, which contains the desired position and velocity at t_f and the calculated state $\mathbf{R}(t_f)$:

$$E(\boldsymbol{\psi}) = \left|\mathbf{R}_f - \mathbf{R}(t_f)\right|^2 \tag{9}$$

Using an iterative procedure to minimize $E(\boldsymbol{\psi})$ as a function of $\boldsymbol{\psi}(0)$ by a steepest gradient descent method (see Appendix C), the auxiliary vector $\boldsymbol{\psi}(0)$ is iterated until the error $E(\boldsymbol{\psi})$ has become smaller than a predefined small positive value ε. When $E(\boldsymbol{\psi}) < \varepsilon$, the corresponding auxiliary vector $\boldsymbol{\psi}(0)$ results in a movement trajectory with minimum change of joint torques, which approaches the desired end state $\mathbf{R}_f$ arbitrarily closely.

2.3 Setup of the model

In order to show the effects of adding approach constraints, we simulated movements with various combinations of approach constraints. The model arm was represented by a stick figure, having two joints and two segments (see Fig. 1 for the configuration), with the physical parameters inertia and viscosity obtained from Uno et al. (1989). Simulated movements were restricted to the horizontal plane, without gravitational forces. Because we used a non-redundant effector system, each hand position corresponds to a unique joint-angle configuration. In order to compare the predicted movements with observed movements accurately, physical parameters, like segment length and segment mass, as well as input parameters, like movement time and final velocity and acceleration, were obtained from the experiment that is described next.

2.4 Empirical test

An experiment tuned to the restrictions of the models was conducted, i.e., with the arm constrained to the horizontal plane and supported at two points (forearm and upper arm, see Fig. 1) to avoid gravitational forces. The wrist joint was fixated by a cuff that also supported

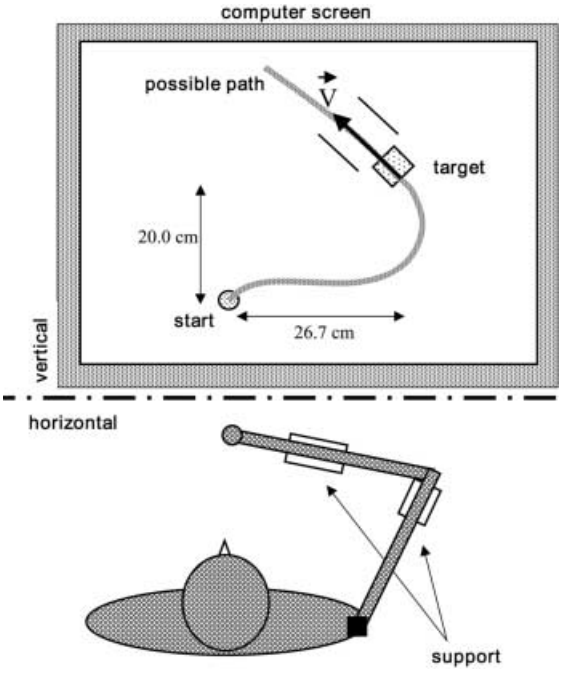

Fig. 1. Participants were seated with their right arm supported horizontally by ropes attached to the ceiling. Real-time feedback of the hand position was given on a computer screen. The hand had to be moved in one fluent motion from the starting position to the target in the direction of the two parallel lines. After each trial the participant was given information on the realized final velocity, the approach angle, and whether the target was hit or missed

the forearm, so that the participants had the same two degrees of freedom as the stick figure in the models. Participants had to make horizontal pointing movements through a virtual target. Targets were projected on a computer screen, as was real-time feedback of the hand position (see Fig. 1). Position data were obtained by means of a three-dimensional infrared motion tracking system (Optotrak 3020; northern Digital Inc., Waterloo, Canada). The movements were sampled at a rate of 100 Hz and with a spatial accuracy of better than 0.1 mm in the x, y, and z directions. The chair on which participants were seated had a straight and high back support, and subjects were requested not to move their trunk. The arm was supported by a swing-like support, attached by a non-elastic rope to the ceiling. The distance between arm and ceiling was 2.5 m, which, in the area where the arm movements took place, resulted in a maximum deviation from the horizontal plane of 0.55 cm, which we considered negligible. At rest, the position of the hand was in the middle between the virtual start and target positions. There were two target positions, 26.7 cm apart, and two starting positions, 20.0 cm closer to the participants. The four of them formed a rectangle. Only diagonal movements from the left starting position to the right target position (rightward movements) and from the right starting position to the left target position (leftward movements) were performed. In the leftward movements, the target had to be approached under $-45°$ and in the rightward movements under 45°, with a final speed of 0.8 m/s. The approach angle was prescribed by two parallel lines. See Fig. 1 for an example of a rightward movement. The same diagonal movements – but ending with zero velocity – had to be performed, at the end of which the hand marker had to stay within a target circle.

Thirteen participants performed twelve leftward and twelve rightward diagonal movements, half of them with the required approach constraints and half ending with zero velocity. There was no prescribed movement time. Participants were asked to make one fluent movement. Six participants started with the zero-velocity condition and seven participants started with the approach-constraints condition. Before each condition, eighteen practice trials were performed in order to learn to move under the required constraints. Leftward and rightward movements were performed in random order. After each trial the subject was given information on the final angle and speed, and whether the target was hit or missed. Maximum allowed errors were 15°, 0.2 m/s, and 3 cm from the middle of the 'bottom' (the side to be hit) of the square, respectively. Trials in which these constraints were not met were repeated immediately. Movement time and final acceleration were not restricted.

Approach angle, final speed, final acceleration, and the movement time of observed trajectories, averaged over the six replications, were used as input parameters for both the minimum-jerk and joint-torque model. For the minimum torque-change model, final velocity and final acceleration were first recalculated into angular velocity and acceleration in the elbow and shoulder joints. As input for the minimum torque-change model, arm length and body weight were also measured. Segment mass and center of mass were determined as a percentage of body weight and arm length, respectively.

Measured as well as simulated trajectories were resampled to 100 equidistant positions along the trajectory. The six replications of each movement condition executed by each participant were averaged. For each trajectory (mean observed and modeled) the curvature was calculated. Curvature was defined as 1/radius (m) of circles fitted to a shifting window of three data points along the trajectory. To compare curvature of leftward and rightward movements, negative curvature was defined as rotating clockwise for rightward movement and anti-clockwise for leftward movements. The percentage trajectory length with negative curvature and peak curvature was calculated and by means of a students t-test differences between leftward and rightward movements were tested (one-tailed, within subject).

3 Results

We will first explain the results of our simulations in Fig. 2, and the resemblances and differences between the sets of trajectories simulated with the two models. In the second part of this section we will compare the simulated trajectories with the measured trajectories.

Figure 2 shows, from top to bottom, simulated minimum-jerk trajectories, simulated minimum torque-change trajectories, and measured trajectories, with

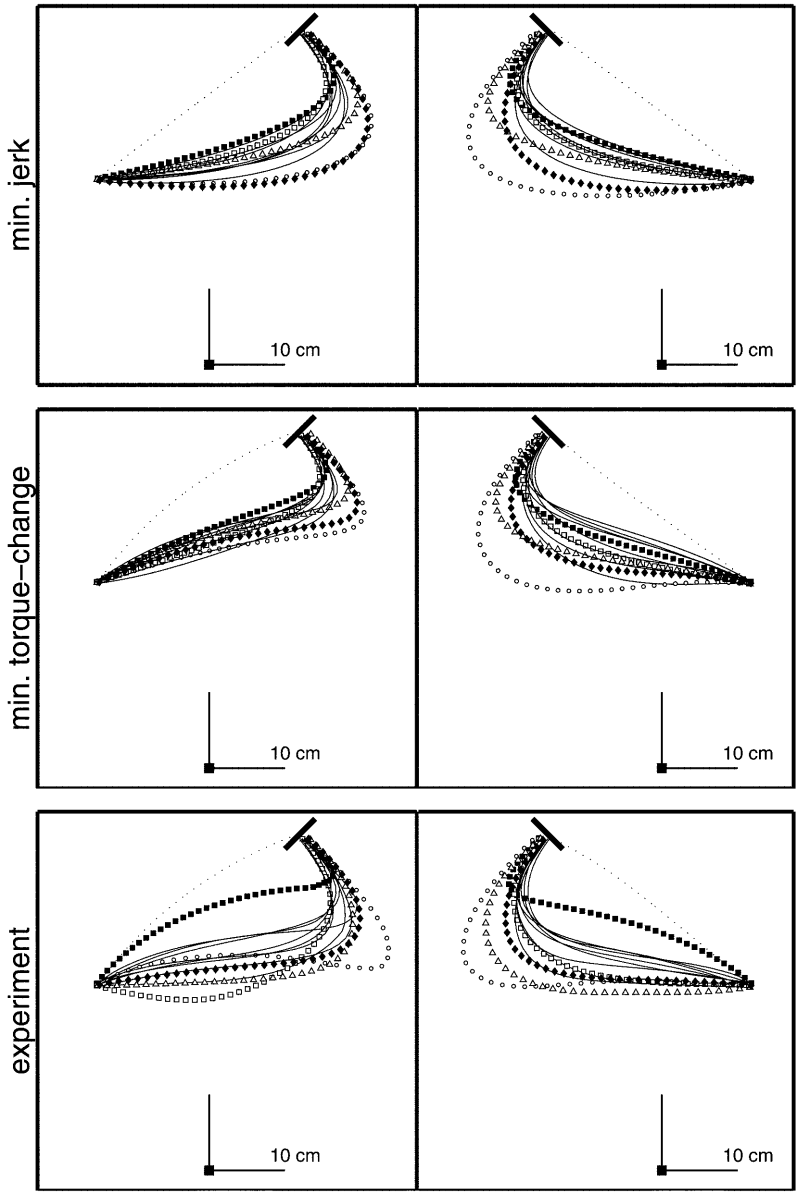

Fig. 2. Simulated minimum-jerk trajectories (*top two panels*), minimum torque-change trajectories (*middle two panels*), and observed trajectories (*bottom two panels*) of 13 participants. Observed trajectories are averaged over six replications. Trajectories with roughly the same shape are shown with *solid lines*, whereas clearly deviating trajectories are represented with a separate line style. Identical line styles in the different panels belong to the same participant. The *thick solid line* indicates the position and orientation of the target square. The *dotted line* represents the ending-with-zero-velocity condition. The shoulder is positioned at the *black square*

leftward movements in the right panels and rightward movements in the left panels. Each curve represents data for one subject. The measured trajectories in the bottom two panels are the mean trajectories of each participant, averaged over the six replications. The simulated trajectories for each subject were obtained with measured initial and final position, final velocity and acceleration, and movement time (all averaged over the six trials) as constraints for the model. The thick line shows the position of the target, which had to be approached perpendicularly with a final speed of 0.8 m/s. The black square shows the average position of the shoulder. Trajectories with roughly the same shape are shown with solid lines, whereas clearly deviating trajectories are represented by a separate line style. The measured movement trajectories in the bottom-left (-right) panel in Fig. 2 should be compared with the simulated trajectories in the upper- and middle-left (-right) panels in Fig. 2. Identical line styles in the different panels belong to the same participant. For comparison, the movement trajectories for the condition with final velocity zero is shown – averaged over replications and participants – by the dotted lines.

3.1 Simulated trajectories

For the simulated trajectories, each line represents a trajectory modeled with the mean observed approach constraints, final acceleration, and movement time (averaged over the six replications) for each participant and, for the minimum torque-change model, with the physical parameters obtained from that participant. To get an impression of magnitudes and inter-subject variability of these input parameters, see Table 1. The approach constraints (target location, angle, and speed) are symmetric along the mid-sagittal plane. The final acceleration, however, appears to be higher for leftward

Table 1A,B. Mean input parameters used for both models, derived from observed trajectories, for leftward and rightward movements separately. Also the between-subject SD is given, except for the starting and target position which were always the same. The direction of the velocity, α_{Vf}, and the direction of the acceleration, α_{Af}, are given as angles with the sagittal vector

Parameter	Leftwards	Rightwards
(A) Parameters used in both models		
Starting position x, y (cm)	44.3, 15.1	17.7, 15.1
Target position x, y (cm)	17.7, 35.1	44.3, 35.1
V_f (m/s)*	0.74 ± 0.05	0.72 ± 0.06
A_f (m/s^2)*	1.99 ± 0.49	1.51 ± 0.37
α_{Vf} (degrees)	−42.1 ± 3.9	44.2 ± 4.3
α_{Af} (degrees)	−82.2 ± 24.6	81.9 ± 24.8
Movement time (s)	0.91 ± 0.19	0.96 ± 0.23
(B) Additional parameters used for the minimum torque-change model. These are the same for leftward and rightward movements		
	Upper arm (shoulder)	Forearm (elbow)
Shoulder position x (cm)	32.6 ± 4.7	–
Shoulder position y (cm)	−9.3 ± 5.3	–
Segment length (cm)	30.2 ± 1.9	33.3 ± 2.2
Segment mass (kg)	1.12 ± 0.22	1.62 ± 0.32
SCM** – distal joint (cm)	13.3 ± 0.9	14.3 ± 1.0
Inertia (kg · m^2)	0.065	0.100
Viscosity (kg · m^2/s)	0.08	0.08

* For the minimum torque-change model V_f and A_f were recalculated into angular velocity and acceleration at the shoulder and elbow joint
** SCM = Segment center of mass

movements that for rightward movements (within-subject, $df = 12, t = 4.09, P < 0.01$). So, although the task was symmetric, the execution is not symmetric.

Without any constraints for approaching the target, the measured and predicted movement trajectories are straight or slightly curved. With the approach constraints, movement trajectories become more curved with a high curvature near the end of a movement. At first glance, both the minimum-jerk and the minimum torque-change model seem to produce movement trajectories, which are close to the measured trajectories. Both the simulated and measured trajectories demonstrate a high curvature near the end of a movement for the approach constraints. Although the approach constraint only applies to the final part of the movement, trajectories for movements with and without an approach constraint deviate from the very beginning, indicating that the constraint at the end of the movement affects the entire movement trajectory.

According to the minimum-jerk model, movement trajectories are programmed in world coordinates, which implies that, if the approach constraints are symmetric, the leftward and rightward trajectories are also symmetric in workspace, independently from the joint excursions that are needed for the movement. Due to inter- and intra-individual differences in final velocity and final acceleration, there are some small differences for leftward and rightward movements, but the global shape of leftward and rightward movements is similar.

Minimum torque-change trajectories, on the other hand, are not symmetric when the configurations of starting and target position and approach angle are symmetric in workspace. For example, the curve at the end of the rightward movements (middle-left panel) is sharper (higher peak curvature) than at the end of the leftward movements (middle-right panel). The reason for this difference between both models is that the minimum torque-change model optimizes the trajectories in joint space and depends on the specific joint excursions bringing about that particular end-effector trajectory.

A second difference between the trajectories generated by the two models under the presently investigated approach constraints is that minimum-jerk trajectories are either convex or concave, with a constant sign of the curvature. Minimum torque-change trajectories, however, are often S-shaped, i.e., they reveal a change of sign of the curvature and thus have an inflection point, which, for example, can be seen in some of the rightward movements (middle-left panel). Eleven out of 13 simulated rightward movements were S-shaped and 12 out of 13 leftward movements.

3.2 Comparison between measured and simulated trajectories

Now we will compare the characteristics of the simulated and measured trajectories. First of all, experimental trajectories look qualitatively similar to the simulated trajectories, with the highest curvature near the end of the movement. In order to compare the simulated and measured trajectories in more detail with respect to the above-mentioned asymmetry and S-shape, we calculated the maximum deviation, the percentage of the trajectory with negative curvature, and peak curvature. The maximum deviation is the largest excursion of each trajectory relative to the straight line that connects the start and target position. Figure 3 shows a scatter plot of the model predictions of this maximum distance vs.

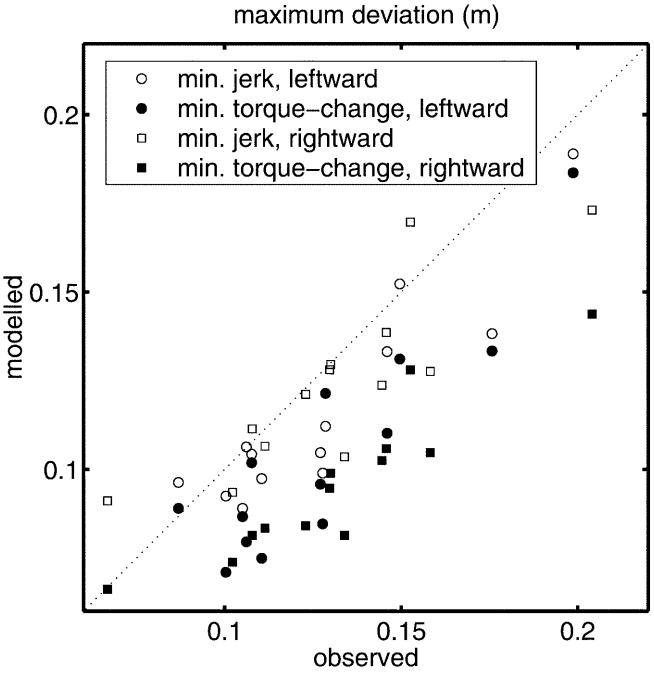

Fig. 3. Scatter plot of the maximum perpendicular deviation relative to the straight line between start and target for the simulated trajectories, vs. that for the observed movement trajectories

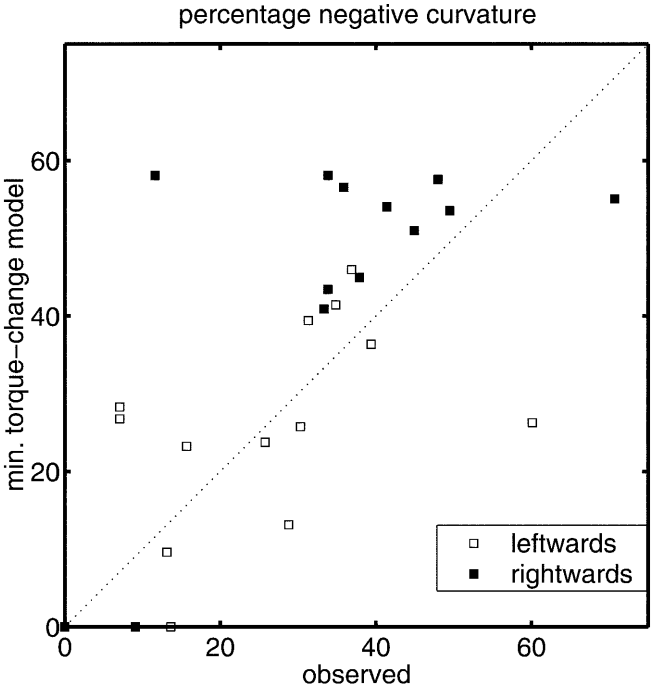

Fig. 4. Scatter plot of the percentage of trajectory length with negative curvature for the minimum torque-change model, vs. the observed percentage

observed distances for each subject for both models and for the data for leftward and rightward movements marked differently. The symbols in Fig. 3 tend to fall below the line with a slope equal to one, indicating that both models predict a lower maximum deviation than observed, which, except for leftward minimum-jerk trajectories, was confirmed by a *t*-test (within-subject, $df = 12$; $t = 1.62$, not significant and $t = 3.17$, $P < 0.01$ for left- and rightward minimum-jerk versus observed trajectories, respectively; $t = 5.88$, $P < 0.01$ and $t = 8.30$, $P < 0.01$ for left- and rightward minimum torque-change versus observed trajectories, respectively). Despite the systematically smaller deviation from a straight line between starting and target position of both models, a Spearman's rank-difference correlation revealed that the order of maximum distances of the measured trajectories and that of the simulated trajectories based upon the minimum torque-change model, was highly correlated ($\rho = 0.80$ and $\rho = 0.93$, $n = 13$, $P < 0.01$) for leftward and rightward movements, respectively. A similar correlation was found when comparing the order of maximum distances of the measured trajectories and the simulated trajectories based upon the minimum-jerk model ($\rho = 0.69$ and $\rho = 0.81$, $n = 13$, $P < 0.01$) for leftward and rightward movements, respectively. Since both models predicted lower maximum deviations than measured, and since the order of maximum deviations predicted by both models coincided with that of the measured trajectories, this variable cannot distinguish between the two models.

As indicated above, a clear difference between trajectories simulated with the two models is the presence or absence of an S-shape in the movement trajectories. Both for the leftward and rightward observed movements, 12 out of 13 trajectories were S-shaped. As indicated above, the minimum-jerk model predicted unimodally-curved trajectories. Consequently, the observed frequency of S-shaped trajectories is at odds with the minimum-jerk model (sign-test, $n = 13$, $P < 0.01$).

Figure 4 shows a scatter plot of the percentage of trajectory length that is negatively curved according to the minimum torque-change model, vs. the observed percentage for each subject. For the measured trajectories, this percentage varies between 0 and 72%, which is about the range for the minimum torque-change trajectories. For leftward movements, the percentage of the observed trajectory length having negative curvature correlates positively with that of the trajectories simulated with the minimum torque-change model (Spearman's, $\rho = 0.48$, $n = 13$, $P < 0.05$). For the rightward movements this correlation did not reach significance ($\rho = 0.40$, $n = 13$, $P = 0.09$). The predicted asymmetry for left- and rightward movements by the minimum torque-change model is clearly visible for this parameter. Figure 4 shows that for rightward movements a larger part is negatively curved than for leftward movements (within-subject, $t = -2.722$, $df = 12$, $P < 0.01$). The same was found for minimum torque-change trajectories (within-subject $t = -4.944$, $df = 12$, $P < 0.01$). The reader should notice that symbols in Fig. 4 near the dotted line with a slope of one stand for perfect minimum torque-change trajectories, whereas symbols that are located above and left of this line stand for observed trajectories that have less negative curvature than predicted by the minimum torque-change model. On the other hand, the symbols that are below and right of the

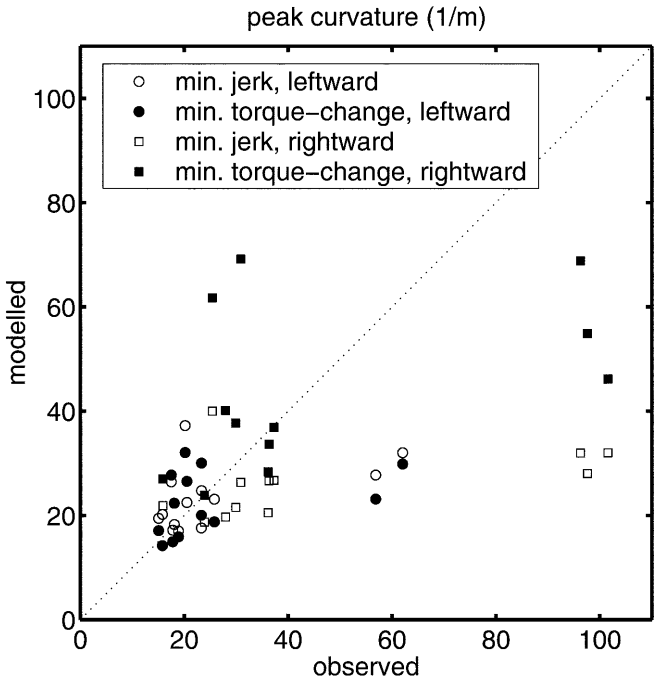

Fig. 5. Scatter plot of simulated peak curvature vs. observed peak curvature

dotted line with slope one stand for trajectories that have exaggerated S-shapes. The right-most filled square and also the right-most open square in Fig. 4, for example, belong to the same participant, whose observed trajectories (filled squares in the bottom panels of Fig. 2) have much more negative curvature than the trajectories simulated with the minimum torque-change model (filled squares in the middle two panels in Fig. 2).

Another measure that illustrates the asymmetry between leftward and rightward movements is peak curvature, as can be seen in Fig. 5. Observed rightward movements have a higher peak curvature than leftward movements (within-subject, $t = -5.162$, $df = 12$, $P < 0.01$), as is also predicted for minimum torque-change trajectories (within-subject, $t = -6.628$, $df = 12$, $P < 0.01$). Although the minimum-jerk model generally predicts symmetric trajectories, the left- and rightward minimum-jerk trajectories have different peak curvatures for the minimum-jerk model as well (within-subject, $t = -2.77$, $df = 12$, $P < 0.05$), due to the asymmetric input parameters.

In summary, we have shown that the S-shapes and asymmetry predicted by the minimum torque-change model are also present in the observed trajectories.

4 Discussion

The aim of this study was to investigate the effect of approach constraints on movement trajectories simulated by the minimum-jerk and minimum torque-change model. Flash and Hogan (1987) showed that movements simulated with the constraint that the velocity at the end of the movement is zero have straight trajectories for the minimum-jerk model, while Uno et al. (1989) showed that trajectories ending with zero velocity are in general curved for the minimum torque-change model. However, these predicted trajectories show little resemblance with experimentally observed trajectories (Klein Breteler et al. 1998) when participants are instructed to arrive at the target areas with a certain velocity and under a specific angle. Brenner and Smeets (1995) also found systematic discrepancies between observed trajectories of pointing movements and simulated minimum-jerk trajectories ending at zero velocity.

Incorporating the observed final velocity and approach angle, both in the minimum-jerk and in the minimum torque-change model, resulted in simulated trajectories (Fig. 2) that are clearly different from simulated trajectories ending with zero velocity. The high curvature that was observed at the final part of the movement trajectories with the endpoint constraints is also present in trajectories simulated with both models. This demonstrates that approach constraints need to be taken into account in order to increase our understanding of the shapes of movement trajectories. Instead of only theoretical movements, characterized by starting and ending at standstill, more realistic movements can be investigated in this way.

When comparing the effects of approach constraints on simulated trajectories, the trajectories simulated with the minimum torque-change model were more similar to the observed trajectories than the trajectories simulated with the minimum-jerk model. The S-shape and the asymmetry between leftward and rightward movements as observed in the experimental trajectories were also found in trajectories predicted by the minimum torque-change model. S-shapes never occur for minimum-jerk trajectories, and the small asymmetry in the minimum-jerk trajectories can be fully explained by the asymmetric final acceleration for left- and rightward movements, which serves as an input parameter.

The results in this paper indicate that the observed trajectories look most like the minimum torque-change trajectories. The minimum torque-change model implies planning in joint-space. Therefore, our results can be interpreted as evidence for movement planning in intrinsic coordinates. We used the minimum-jerk and minimum torque-change models as examples of trajectory-formation models that claim that when subjects are performing basic pointing movements, they try to minimize certain movement costs, in workspace coordinates or in joint-torque space, respectively. In order to evaluate the effects of approach constraints on trajectory formation, we used the two models without the intention to discriminate between the relative powers of these specific models as the primary goal of our research. Recently, several variations have been presented as an alternative to the minimum torque-change model, such as the minimum muscle-tension model (Dornay et al. 1996) and the minimum-commanded torque-change model (Nakano et al. 1999). From a biological point of view, a model stating that movements are optimized in muscle space may seem to be more plausible than a model stating that movements are optimized in joint

space. However, simulating an arm movement with a minimum muscle-tension change model requires a lot more model parameters, such as optimum muscle length and muscle attachment sites, which introduces many degrees of freedom. Dornay et al. (1996) showed that minimum muscle-tension change trajectories show the same S-shapes as minimum torque-change trajectories, which was also shown in the study of Nakano et al. (1999). Dornay et al. (1996) stated that "the predictions of the minimum joint-torque change model were at least as good, or even a little better, than the predictions of the minimum muscle-tension change model". Therefore we have restricted ourselves to the minimum torque-change model as a good representative for the class of models operating in intrinsic coordinates.

The extent to which variables like jerk or torque change are taken into account in movement planning processes alone or, alternatively, in influencing trajectory characteristics during movement execution, remains an open question. The currently investigated movements took about one second, which gave our subjects ample time to adjust their movements in real time. The systematic difference that we found between on the one hand the model-based predictions of the maximum deviations from the straight line between start and end of the movements and on the other hand the observed maximum deviations, indeed suggest that processes taking place during movement execution may have had an impact on the actual shape of the observed trajectories. However, the degree to which the minimum torque-change model accurately accounted for the other two criteria involved in the current model evaluation, i.e., the presence or absence of S-shapes and the systematic curvature variations, suggests, in our view, that it is likely that important aspects of motion planning are addressed by the models investigated.

As explained in Sect. 1, several past experiments have discussed the nature of movement trajectories, being straight or curved (see, e.g., Morasso 1981; Atkeson and Hollerbach 1985). In this study we report that movement trajectories for movements with end point constraints are S-shaped. This study does not want to infer any direct conclusions based on these S-shaped trajectories. However, the fact that the minimum torque-change model, which operates in joint-torque space, gives the best fit to the observed movement trajectories, suggests in our view that an intrinsic frame of reference is involved in producing these S-shaped trajectories.

Besides the fact that subjects might be capable of planning movements both in workspace and in intrinsic space, depending on the particular weights of the constraints of a particular motor task (see, e.g., Rosenbaum et al. 1995, 1996), it is also possible that in both spaces several parameters are optimized at the same time, thus preventing any parameter being too far from its optimum value, as suggested by Kawato (1996). A trajectory would in that case be some combination of minimum-jerk and minimum torque-change trajectories, making it difficult to determine quantitatively the relative power of the two models. S-shapes and asymmetries could still be visible in such combined trajectories. For the class of movements investigated here, we conclude that at least some optimization in intrinsic space took place.

Appendix A

In this appendix we present the calculation of angular accelerations for the shoulder and elbow. The angular accelerations in both joints are the third and fourth components of the six-dimensional vector $\mathrm{d}\mathbf{R}/\mathrm{d}t$, as given in (7). For this purpose we rewrite the dynamics equation (5) in the text. To make the equation simpler, it is first broken into chunks:

$$a_1(\theta_2) = I_1 + I_2 + 2M_2L_1S_2\cos\theta_2 + M_2L_1^2$$

$$b_1(\theta_2) = I_2 + M_2L_1S_2\cos\theta_2$$

$$c_1(\dot\theta_1, \dot\theta_2) = -M_2L_1S_2(2\dot\theta_1 + \dot\theta_2)\dot\theta_2\sin\theta_2 + \beta_1\dot\theta_1$$

$$a_2(\theta_2) = I_2 + M_2L_1S_2\cos\theta_2$$

$$b_2 = I_2$$

$$c_2(\dot\theta_1, \dot\theta_2) = M_2L_1S_2\dot\theta_1^2\sin\theta_2 + \beta_2\dot\theta_2$$

$$D(\theta_2, \dot\theta_1, \dot\theta_2) = a_2b_1 - a_1b_2$$

With the help of these chunks and with (5), the angular accelerations can be described as a function of θ_1, θ_2, $\dot\theta_1$, $\dot\theta_2$, and the joint torques T_1 and T_2:

$$\ddot\theta_1 = -\frac{b_1c_2}{D} + \frac{b_2c_1}{D} - \frac{b_2}{D}T_1 - \frac{b_1}{D}T_2$$

$$\ddot\theta_2 = \frac{a_1c_2}{D} - \frac{a_2c_1}{D} + \frac{a_2}{D}T_1 - \frac{a_1}{D}T_2$$

Appendix B

In this appendix we explain how the elements of the 6×6 matrix $\partial\mathbf{f}/\partial\mathbf{R}$ are calculated. First the chunks mentioned in Appendix A are differentiated with respect to the parameter in the denominator. The first derivatives of the chunks to θ_2 are:

$$a_1^{\theta_2} \equiv \frac{\partial a_1}{\partial\theta_2} = -2M_2L_1S_2\sin\theta_2$$

$$b_1^{\theta_2} \equiv \frac{\partial b_1}{\partial\theta_2} = -M_2L_1S_2\sin\theta_2$$

$$c_1^{\theta_2} \equiv \frac{\partial c_1}{\partial\theta_2} = -M_2L_1S_2(2\dot\theta_1 + \dot\theta_2)\dot\theta_2\cos\theta_2$$

$$a_2^{\theta_2} \equiv \frac{\partial a_2}{\partial\theta_2} = b_1^{\theta_2}$$

$$b_2^{\theta_2} \equiv \frac{\partial b_2}{\partial \theta_2} = 0$$

$$c_2^{\theta_2} \equiv \frac{\partial c_2}{\partial \theta_2} = M_2 L_1 S_2 \dot{\theta}_1^2 \cos\theta_2$$

$$D^{\theta_2} \equiv \frac{\partial D}{\partial \theta_2} = -2M_2^2 L_1^2 S_2^2 \cos\theta_2 \sin\theta_2$$

With the help of these partial derivatives $\partial \mathbf{f}_3/\partial \mathbf{R}_2$ and $\partial \mathbf{f}_4/\partial \mathbf{R}_2$ can be calculated:

$$\frac{\partial \ddot{\theta}_1}{\partial \theta_2} = \frac{-(b_1^{\theta_2} c_2 + b_1 c_2^{\theta_2})D - b_1 c_2 D^{\theta_2}}{D^2} + \frac{b_2(c_1^{\theta_2} D - c_1 D^{\theta_2})}{D^2} - \frac{b_2 z_1 D^{\theta_2}}{D^2} + \frac{z_2(b_1^{\theta_2} D - b_1 D^{\theta_2})}{D^2}$$

$$\frac{\partial \ddot{\theta}_2}{\partial \theta_2} = \frac{(a_1^{\theta_2} c_2 + a_1 c_2^{\theta_2})D - a_1 c_2 D^{\theta_2}}{D^2} - \frac{(a_2^{\theta_2} c_1 + a_2 c_1^{\theta_2})D - a_2 c_1 D^{\theta_2}}{D^2} + \frac{z_1(a_2^{\theta_2} D - a_2 D^{\theta_2})}{D^2} - \frac{z_2(a_1^{\theta_2} D - a_1 D^{\theta_2})}{D^2}$$

With the help of the partial derivatives

$$\frac{\partial c_1}{\partial \dot{\theta}_1} \equiv c_1^{\dot{\theta}_1} = -2M_2 L_1 S_2 \dot{\theta}_2 \sin\theta_2 + \beta_1$$

$$c_2^{\dot{\theta}_1} \equiv \frac{\partial c_2}{\partial \dot{\theta}_1} = 2M_2 L_1 S_2 \dot{\theta}_1 \sin\theta_2$$

the elements $\partial \mathbf{f}_3/\partial \mathbf{R}_3$ and $\partial \mathbf{f}_4/\partial \mathbf{R}_3$ can be calculated:

$$\frac{\partial \ddot{\theta}_1}{\partial \dot{\theta}_1} = -\frac{b_1 c_2^{\dot{\theta}_1}}{D} + \frac{b_2 c_1^{\dot{\theta}_1}}{D}$$

$$\frac{\partial \ddot{\theta}_2}{\partial \dot{\theta}_1} = \frac{a_1 c_2^{\dot{\theta}_1}}{D} - \frac{a_2 c_1^{\dot{\theta}_1}}{D}$$

With the partial derivatives

$$c_1^{\dot{\theta}_2} \equiv \frac{\partial c_1}{\partial \dot{\theta}_2} = -M_2 L_1 S_2 (2\dot{\theta}_1 + 2\dot{\theta}_2) \sin\theta_2$$

$$c_2^{\dot{\theta}_2} \equiv \frac{\partial c_2}{\partial \dot{\theta}_2} = \beta_2$$

the elements $\partial \mathbf{f}_3/\partial \mathbf{R}_4$ and $\partial \mathbf{f}_4/\partial \mathbf{R}_4$ can be calculated:

$$\frac{\partial \ddot{\theta}_1}{\partial \dot{\theta}_2} = -\frac{b_1 c_2^{\dot{\theta}_2}}{D} + \frac{b_2 c_1^{\dot{\theta}_2}}{D}$$

$$\frac{\partial \ddot{\theta}_2}{\partial \dot{\theta}_2} = \frac{a_1 c_2^{\dot{\theta}_2}}{D} - \frac{a_2 c_1^{\dot{\theta}_2}}{D}$$

The elements in the fifth and sixth column of the 6×6 matrix $\partial \mathbf{f}/\partial \mathbf{R}$ are simply given by:

$$\frac{\partial \ddot{\theta}_1}{\partial T_1} = -\frac{b_2}{D}$$

$$\frac{\partial \ddot{\theta}_2}{\partial T_1} = \frac{a_2}{D}$$

$$\frac{\partial \ddot{\theta}_1}{\partial T_2} = \frac{b_1}{D}$$

$$\frac{\partial \ddot{\theta}_2}{\partial T_2} = -\frac{a_1}{D}$$

Appendix C: The iterative optimization procedure

The optimization procedure to minimize the error $E(\boldsymbol{\psi}(0))$ in (9) is performed as follows. For a given initial vector $\boldsymbol{\psi}(0)$, the error $E(\boldsymbol{\psi}(0))$ is calculated. In addition, the error is calculated for small perturbation $\boldsymbol{\psi}'(0) = \boldsymbol{\psi}(0) + \varepsilon \mathbf{e}_i$, where $\mathbf{e}_i$ is a unit vector ($1 \leq i \leq 6$). This gives a 6×6 error matrix $\mathbf{S}(\boldsymbol{\psi}, \varepsilon)$ is calculated:

$$\mathbf{S}(\boldsymbol{\psi}, \varepsilon) = ((E(\boldsymbol{\psi} + \varepsilon \mathbf{e}_1) - E(\boldsymbol{\psi}))\ \varepsilon, \cdots, (E(\boldsymbol{\psi} + \varepsilon \mathbf{e}_6) - E(\boldsymbol{\psi}))\ \varepsilon)$$

Subsequently, a new initial vector $\boldsymbol{\psi}(0)$ is calculated according to the following formula:

$$\boldsymbol{\psi}(0)^{k+1} = \boldsymbol{\psi}(0)^k - \gamma \mathbf{S}(\boldsymbol{\psi}(0), \varepsilon)^{-1} E(\boldsymbol{\psi}(0)^k)$$

This new initial $\boldsymbol{\psi}(0)$ results in a movement that is closer to the final target position and target velocity than the former initial $\boldsymbol{\psi}(0)$. The scalar γ is a gain factor that guarantees proper convergence to smaller errors $E(\boldsymbol{\psi}(0))$ without fluctuations.

References

Atkeson CG, Hollerbach JM (1985) Kinematic features of unrestrained vertical arm movements. J Neurosci 5: 2318–2330

Boessenkool JJ, Nijhof EJ, Erkelens CJ (1998) A comparison of curvatures of left and right hand movements in a simple pointing task. Exp Brain Res 120: 369–376

Brenner E, Smeets JBJ (1995) Moving one's finger to a visually specified position: target orientation influences the finger's path. Exp Brain Res 105: 318–320

Dornay M, Uno Y, Kawato M, Suzuki R (1996) Minimum muscle-tension change trajectories predicted by using a 17-muscle model of the monkey's arm. J Motor Behav 28: 83–100

Flash T, Hogan N (1985) The coordination of arm movements: an experimentally confirmed mathematical model. J Neurosci 5: 1688–1703

Flash T (1987) The control of hand equilibrium trajectories in multi-joint arm movements. Biol Cybern 57: 257–274

Haggard P, Richardson J (1996) Spatial patterns in the control of human arm movement. J Exp Psychol Hum Percep Perform 22: 42–62

Kawato M (1996) Bidirectional theory approach to integration. In: Inui T, McClelland JL (eds) Attention and performance XVI:

information integration in perception and communication. MIT Press, Cambridge, Mass., pp 335–367
Klein Breteler MD, Meulenbroek RGJ, Gielen CCAM (1998) Geometric features of workspace and joint-space paths of 3D reaching movements. Acta Psychol (Amst) 100: 37–53
Morasso P (1981) Spatial control of arm movements. Exp Brain Res 42: 223–227
Nakano E, Imamizu H, Osu R, Uno Y, Gomi H, Yoshioka T, Kawato M (1999) Quantitative examinations of internal representations for arm trajectory planning: minimum commanded torque change model. J Neurophysiol 81: 2140–2155
Rosenbaum DA, Loukopoulos LD, Meulenbroek RGJ, Vaughan J, Englebrecht S (1995) Planning reaches by evaluating stored postures. Psychol Rev 102: 28–67
Rosenbaum DA, Loukopoulos LD, Engelbrecht SE, Meulenbroek RGJ, Vaughan J (1996) Integration of extrinsic space and motor space. In: Inui T, McClelland JL (eds) Attention and performance XVI: information integration in perception and communication. MIT Press, Cambridge, Mass., pp 315–333
Smeets JBJ, Brenner E (1999a) A new view on grasping. Motor Control 3: 237–271
Smeets JBJ, Brenner E (1999b) Grip formation as an emergent property. Response to commentaries on ''A new view on grasping''. Motor Control 3: 316–325
Uno Y, Kawato M, Suzuki R (1989) Formation and control of optimal trajectory in human multijoint arm movement. Minimum torque-change model. Biol Cybern 61: 89–101
Van Thiel E, Meulenbroek RGJ, Hulstijn W (1998) Path curvature in workspace and in joint space: evidence for co-existing coordinative rules in aiming. Motor Control 2: 331–351